

Mapping tuberculosis fatalities by region and age group in South Korea: A dataset for targeted health policy optimization

Yongsung Kwon¹, Deok-Sun Lee^{2*}, Mi Jin Lee^{3*}, and Seung-Woo Son^{1,4,*}

¹Department of Applied Artificial Intelligence, Hanyang University, Ansan 15588, Korea

²School of Computational Sciences, Korea Institute for Advanced Study, Seoul 02455, Korea

³Department of Physics, Pusan National University, Busan 46241, Korea

⁴Department of Applied Physics, Hanyang University, Ansan 15588, Korea

*Corresponding Author(s): Deok-Sun Lee (deoksunlee@kias.re.kr), Mi Jin Lee (mijinlee@pusan.ac.kr), Seung-Woo Son (sonswoo@hanyang.ac.kr)

ABSTRACT

In South Korea, age-disaggregated tuberculosis (TB) data at the district level are not publicly available due to privacy constraints, limiting fine-scale analyses of healthcare accessibility. To address this limitation, we present a high-resolution, district-level dataset on tuberculosis (TB) fatalities and hospital accessibility in South Korea, covering the years 2014 to 2022 across 228 districts. The dataset is constructed using a reconstruction method that infers age-disaggregated TB cases and fatalities at the district level by integrating province-level age-specific statistics with district-level spatial and demographic data, enabling analyses that account for both spatial heterogeneity and age structure. Building on an existing hospital allocation framework, we extend the objective function to an age-weighted formulation and apply it to the reconstructed dataset to minimize TB fatalities under different age-weighting schemes. We demonstrate that incorporating age structure can give rise to distinct optimized hospital allocation patterns, even when the total number of minimized fatalities is similar, revealing trade-offs between efficiency and demographic targeting. In addition, the dataset supports temporal analyses of TB burden, hospital availability, and demographic variation over time, and provides a testbed for spatial epidemiology and optimization studies that require high-resolution demographic and healthcare data.

Introduction

Tuberculosis (TB) remains one of the leading causes of infectious disease mortality worldwide, with an estimated 1.3 million deaths annually^{1,2}. Despite long-term global efforts to control the disease, substantial regional disparities in TB incidence and outcomes persist^{3,4}. Within the Organization for Economic Co-operation and Development (OECD), South Korea presents a notable case: it consistently reports over 10,000 new TB cases annually and ranks second in TB incidence and fifth in TB-related mortality among OECD countries⁵. This combination of persistently high burden and comprehensive public health surveillance distinguishes Korea from most high-income countries with small numbers.

South Korea maintains a fully digitized public health reporting system in which annual statistics on TB patients, fatalities, and healthcare infrastructure are collected and released at the administrative district level^{6,7}, covering over 200 districts nationwide. In such data-rich settings, where disease surveillance is systematically curated and released with high spatial coverage, the integration of population and geographic information enables detailed analyses of spatial inequality and accessibility in urban systems^{3,4,8–10}. South Korea provides a representative example of this environment, allowing us to examine hospital distribution and accessibility patterns in urban infrastructure using established spatial and optimization-based approaches^{3,11–14}.

More broadly, the spatial distribution of public infrastructure has been studied as a generic feature of urban systems, where facility density scales with population density^{10,12,13,15,16}. In the context of healthcare, such spatial organization can influence not only average accessibility but also the robustness of service provision under uneven demand or localized constraints, as observed in other infrastructure systems^{9,17}. However, in practice, privacy constraints prevent most existing analyses from accessing disease data that are jointly disaggregated by age and administrative district at fine spatial resolution, limiting their ability to capture demographic heterogeneity in disease outcomes.

Age is a critical determinant of TB disease severity^{5,18}. Older individuals are more likely to experience fatal outcomes and may face structural barriers to early diagnosis or continuous treatment^{19,20}. In South Korea, TB fatalities are heavily concentrated among individuals aged 70 years and older [Fig. 1(a)], whereas the general population is predominantly concentrated in middle-aged groups, indicating a pronounced mismatch between demographic structure and TB mortality risk that cannot be captured

by age-agnostic models. However, as mentioned above, due to privacy regulations, Korean public health statistics do not provide TB data that are jointly disaggregated by age and higher-spatial-resolution administrative districts (e.g., specific age groups within specific districts)⁶. While province-level age disaggregation is available at lower spatial resolution, this limitation creates a structural data gap that hinders age-aware spatial analysis and equity assessments at the district level, where policy interventions are typically implemented⁶.

To address this gap, we reconstruct a district-level, age-disaggregated dataset of TB patients and fatalities spanning 2014 to 2022. Our method integrates publicly available province-level age distributions with district-level totals through an upscaling procedure, thereby introducing age resolution while preserving spatial fidelity. Because the reconstruction is based solely on aggregated statistics and does not involve individual-level records, it does not increase privacy risks beyond those present in the original data. The reconstructed dataset can also be used as a testbed for evaluating age-aware spatial analyses under realistic administrative constraints. The full reconstruction pipeline and source code are released alongside the dataset, enabling reproducibility and reuse in spatial epidemiology, healthcare accessibility, and infrastructure optimization studies that require both fine spatial resolution and demographic detail.

Furthermore, hospital accessibility plays a central role in disease outcomes, as effective treatment requires early diagnosis and repeated visits to secondary care facilities over extended periods^{2,19,20}. Previous optimization studies have shown that increasing hospital density and accessibility is associated with reduced TB fatalities¹¹. These approaches, however, typically assume uniform vulnerability across patients and do not incorporate age-specific fatality risk, despite strong empirical evidence that TB outcomes vary sharply with age.

Building on this line of work, we extend an existing hospital relocation optimization framework by embedding an age-weighted fatality minimization objective. By explicitly accounting for age-specific vulnerability, the model allows us to examine how demographic structure interacts with spatial allocation under fixed infrastructural constraints. We demonstrate that even when total minimized fatalities are comparable, incorporating age structure can lead to substantially different hospital allocation patterns across districts. By combining district-level data reconstruction with age-aware spatial optimization, this study provides a quantitative framework for analyzing how demographic heterogeneity influences healthcare accessibility and TB fatality outcomes in aging societies.

Background and Motivation

To optimize hospital density for minimizing TB fatalities, a previous study¹¹ formulated the TB fatalities E as a function of hospital density while accounting for human mobility, based on a random-walk model with traps²¹, as follows:

$$E(\vec{\eta}) = \sum_s N_s \phi_s(\eta_s) = \sum_s N_s \exp(-\eta_s/\tilde{\eta}_s), \quad (1)$$

where the hospital density η_s and the fatality rate¹ ϕ_s for district s are defined as $\eta_s \equiv H_s/A_s$ and $\phi_s \equiv D_s/N_s$, where H_s is the number of hospitals, A_s is the district area, and D_s and N_s are the numbers of TB-related deaths and newly reported TB cases, respectively, in a given year. The hospital configuration across all districts is denoted by $\vec{\eta} = (\eta_1, \eta_2, \dots, \eta_s, \dots)$. The characteristic hospital density $\tilde{\eta}_s$, which reflects the medical and infrastructural environment, can be empirically determined by equating the observed fatality rate ($\phi_s \equiv D_s/N_s$) to the modeled form $\phi_s = \exp(-\eta_s/\tilde{\eta}_s)$, yielding $\tilde{\eta}_s = \eta_s/\log(N_s/D_s)$, as reported in the previous study¹¹. Preserving the total number of hospitals, the optimal hospital density of district s is theoretically obtained as $\eta_s^{(\text{opt})} = \tilde{\eta}_s \log(\rho_s/(z\tilde{\eta}_s))$, where $\rho_s = N_s/A_s$ denotes the patient density and z is a Lagrange multiplier. The previous study further demonstrated that the ratio $\eta^{(\text{opt})}/\eta$ between the optimal and current hospital densities strongly depends on the characteristic patient density $\rho_s/\tilde{\eta}_s$ ¹¹.

This modeling framework assumes that the fatality rate ϕ depends solely on the characteristics of each district and therefore does not capture the well-known dependence of TB fatality on patient age^{1,18}. This simplification is primarily due to data limitations: as of 2022, South Korea comprises 228 “si-gun-gu” districts (municipal government level, higher-resolution administrative units), which belong to 17 “si-do” provinces (regional local government level, lower-resolution units). Each province includes as few as 2 districts (Jeju Special Self-Governing Province) and as many as 31 districts (Gyeonggi-do, part of the Seoul metropolitan area). While TB data at the district level are more suitable for statistically robust analysis, age-disaggregated TB data are only available at the province level due to privacy concerns. Figure 1(a) illustrates the age-dependent TB fatality rates for the year 2022. Data provided by the Korea Disease Control and Prevention Agency (KDCA)⁶ and Statistics Korea (KOSIS)⁷ include the number N_t of newly reported TB cases and the number D_t of TB-related deaths for each age group t , aggregated at the province level. As shown in Fig. 1(a), the fatality rate $\phi_t = D_t/N_t$ exhibits substantial variation across age

¹The case fatality rate is generally defined as the proportion of diagnosed patients who die from a disease, but this measure can be biased by undiagnosed cases and unresolved outcomes. For TB, estimates of the total number of cases are known to strongly correlate with the number of newly reported cases. Accordingly, in this study and in previous studies, the fatality rate is approximated by the ratio of TB-related deaths to newly reported TB cases in a given year.

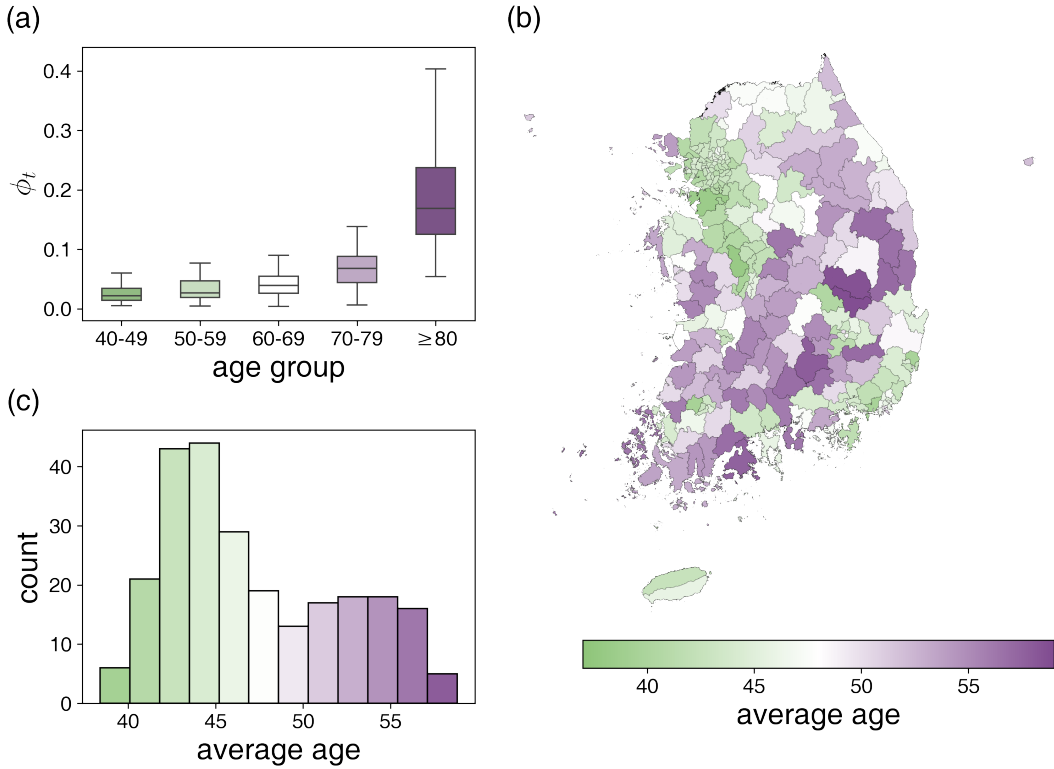


Figure 1. (a) Quartile plots of the fatality rate ϕ_t by age group t across 16 provinces in 2022 (excluding Sejong-si due to the absence of reported fatalities). (b) Average age of the general population across the districts. Metropolitan districts tend to have younger populations, while non-metropolitan districts are characterized by older populations. (c) The distribution of average age displays a heterogeneous pattern in South Korea, indicating an overconcentration of younger individuals in metropolitan areas.

groups, with median values ranging from 0.0219 to 0.1690. Age groups under 40 years are not shown, as they exhibit negligible fatality rates.

In addition to age-related variability, the wide range of fatality rates observed within each age group suggests the presence of substantial spatial heterogeneity. While age-disaggregated TB data are not available at the district level, spatial differences can be indirectly inferred from the age composition of the general population. As shown in Fig. 1(b), metropolitan districts, including the capital city Seoul, tend to have younger average populations than non-metropolitan districts, resulting in a skewed age distribution across regions. This demographic contrast implies that the age composition of TB patients is also likely to vary spatially at the district level. These considerations motivate the need for TB data that jointly capture age structure and spatial resolution, which we address by constructing a higher-resolution, age-inclusive dataset and extending the fatality rate formulation accordingly.

Methods

Raw data sources and spatial resolution

We utilize publicly available datasets reported annually from 2014 to 2022, provided by KDCA⁶ and KOSIS⁷. This study requires age-disaggregated demographic and TB-related information at the district level, the higher-resolution administrative unit. Over this nine-year period, data have been collected for 17 provinces and 228 districts. In contrast to demographic information, such as the number N of newly reported TB cases and the number D of TB-related deaths by age group, non-demographic information, including the number H of hospitals, is available at the district scale. Here, “hospital” refers to a secondary care hospital equipped to provide appropriate treatment for TB. The annual totals of each dataset are summarized in Table 1, and a subset of the data is visualized regionally in Fig. 2.

Year	N	D	H
2014	34 869	2 136	330
2015	32 182	2 018	335
2016	30 892	2 020	339
2017	28 161	1 678	344
2018	26 433	1 657	346
2019	23 821	1 492	354
2020	19 933	1 222	360
2021	18 335	1 324	364
2022	16 264	1 223	374

Table 1. Total annual records of the TB empirical data. The number N of newly reported TB cases and the number D of TB-related deaths are available at the province level due to privacy concerns. The number H of hospitals is provided at the district level. Here “hospital” refers to a secondary care hospital, which is equipped to provide proper treatment for TB.

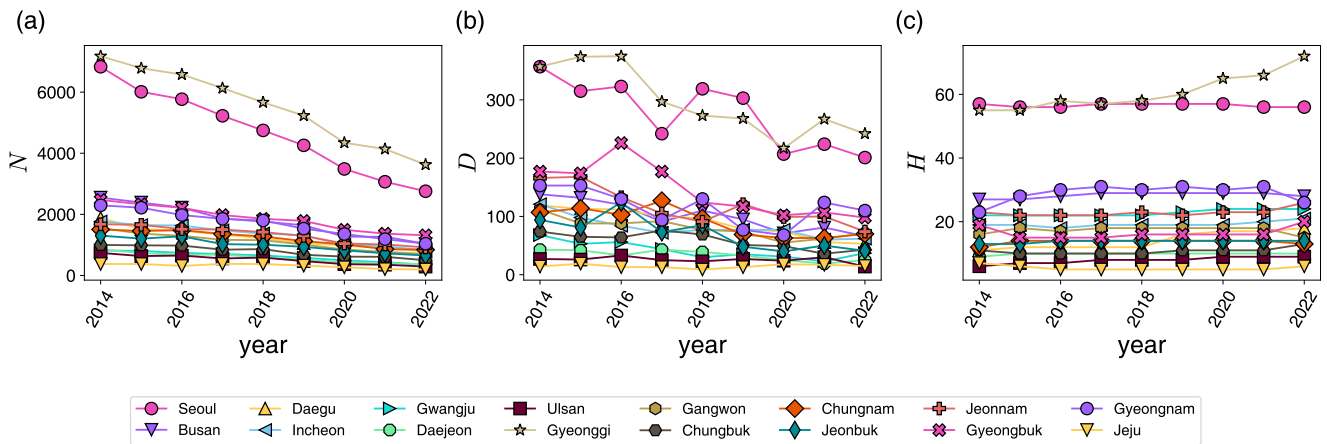


Figure 2. Temporal patterns of the raw data for (a) the number N of newly reported TB cases, (b) the number D of TB-related deaths, and (c) the number H of hospitals. The number of new TB cases and deaths is showing a declining trend. The number of secondary care hospitals is slightly increasing in the Gyeonggi-do region. The 16 provinces are represented by distinct symbols.

Figure 2 shows the temporal patterns of these data for each province separately. Seoul-si and Gyeonggi-do exhibit markedly higher values across all measured quantities than other provinces, reflecting their combined population of nearly half of South Korea’s total population (approximately 22 million out of 50 million). The number N of newly reported TB cases shows a consistent downward trend across all provinces [Fig. 2(a)], and the number D of TB-related deaths also decreases with small fluctuations [Fig. 2(b)], indicating steady nationwide progress toward TB control. The number H of hospitals remains nearly unchanged in most provinces, except for Gyeonggi-do. As a major metropolitan region surrounding the capital city Seoul, Gyeonggi-do has continued to experience population growth driven by suburbanization. This population increase has been accompanied by a growing demand for infrastructure, including hospitals.

To examine the age-group composition of TB cases and fatalities, we measure the fractions $n_{i,t}$ and $d_{i,t}$ of individuals in age group t among newly reported TB cases and TB-related deaths in province i , respectively, as

$$n_{i,t} = N_{i,t}/N_i, \quad d_{i,t} = D_{i,t}/D_i, \quad (2)$$

where $N_i = \sum_t N_{i,t}$ and $D_i = \sum_t D_{i,t}$. Ages are categorized into ten-year groupings. Similarly, the quantities N_t and D_t , used to compute the age-dependent fatality rate ϕ_t shown in Fig. 1(a), are calculated as $N_t = \sum_i N_{i,t}$ and $D_t = \sum_i D_{i,t}$, respectively. The resulting age-group fractions are plotted in Fig. 3. The TB-related fractions n and d , shown in Figs. 3(a) and 3(b), increase monotonically with age. Notably, age dependence is more pronounced for TB-related deaths than for newly reported cases. Moreover, TB deaths in Fig. 3(b) contrast with the age distribution of the general population shown in Fig. 3(c): although the population in South Korea is primarily concentrated in the 40–60 year age range, TB-related deaths are disproportionately concentrated among individuals aged 70 years and older. These observations indicate that the age distribution of TB fatalities deviates systematically from the underlying population structure, emphasizing the need to explicitly account for age-dependent effects in the subsequent analysis.

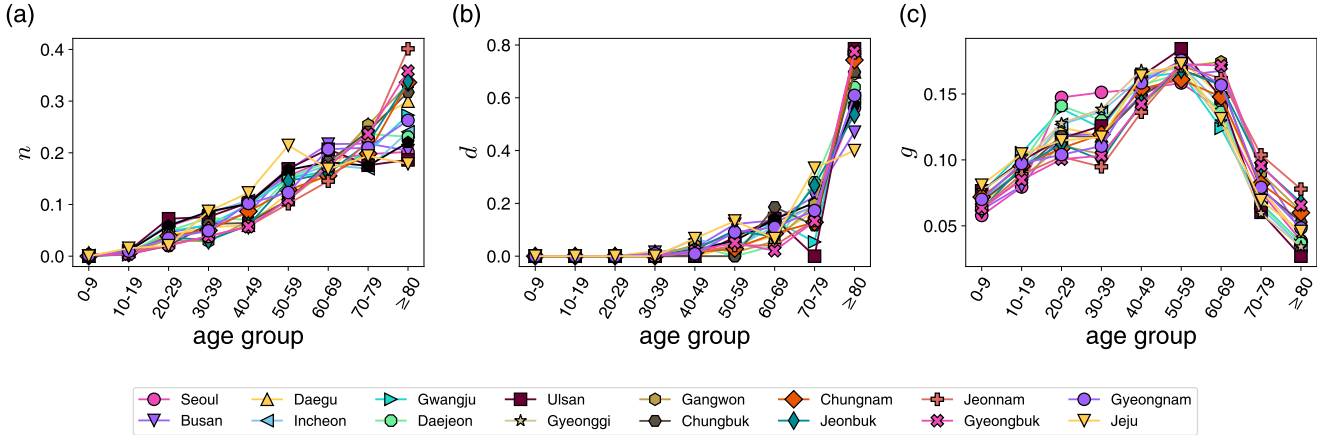


Figure 3. Regional and age-grouped tendency of (a) TB patients fraction n , (b) TB deaths fraction d , and, as a comparison, (c) the general population demographic fraction g for the respective province in 2022. Both the proportion of new TB cases and TB-related deaths tend to increase with age. The 16 provinces are represented by distinct symbols.

Upscaling TB demographic data to high spatial resolution

The raw demographic data related to TB described in the previous subsection are officially available in an age-disaggregated format only at the provincial level. To enable a more fine-grained analysis while maintaining statistical robustness, we develop a method to reconstruct TB case and fatality counts at the district level. Specifically, we assume that the age distributions observed at the provincial level [Figs. 3(a) and 3(b)] also apply to the districts within each province. Then, we can estimate the numbers of TB cases and deaths in district s , belonging to province i , for age group t using Eq. (2) as

$$N_{s,t} \equiv n_{i,t} N_s, \quad D_{s,t} \equiv d_{i,t} D_s, \quad (3)$$

where N_s and D_s denote the age-aggregated numbers of newly reported TB cases and TB-related deaths in district s , respectively, that are available in KDCA and KOSIS. The reconstructed data satisfy $\sum_s' N_{s,t} = N_{i,t}$ and $\sum_s' D_{s,t} = D_{i,t}$, where the primed summation runs over districts s belonging to province i . In this reconstruction framework, the age-group fractions are assumed to be homogeneous within each province, such that $n_{s,t} = n_{i,t}$ for all districts $s \in i$.

Year	S	N	D	H
2014	143	32 322	1 718	328
2015	137	21 683	1 296	312
2016	132	20 207	1 255	306
2017	143	19 427	1 110	330
2018	142	18 145	1 157	334
2019	119	14 318	901	285
2020	116	12 079	736	276
2021	113	10 900	749	262
2022	124	11 789	886	314

Table 2. Summary of annual TB data at the district level available from 2014 to 2022. For each year, the table lists the number S of districts considered, the number N of newly reported TB cases across those districts, the number D of TB-related deaths, and the number H of hospitals. The numbers of newly reported cases N and fatalities D are estimated in an age-disaggregated manner based on province-level age distributions using Eq. (3). All included districts satisfy the conditions of having at least one newly reported TB case ($N \geq 1$), at least one TB-related death among individuals aged 40 years and older ($D \geq 1$), and at least one hospital ($H \geq 1$).

To implement the optimal distribution of hospitals based on the random walk model as in the previous study¹¹, the numbers of TB patients, TB-related deaths, and hospitals of each district are used. We extend this formulation to incorporate age effects using Eq. (3). In addition, as mentioned earlier and shown in Fig. 3(b), the number of TB-related deaths is extremely low (nearly zero) for age groups under 40. Therefore, we exclude age groups under 40, resulting in five age groups being considered:

$t \in \{1, 2, 3, 4, 5\}$ (e.g., $t = 1$ denotes the age group “40–49”). In summary, the subset of data that satisfies these requirements is extracted from the full set of districts and is presented in Table 2. The number of districts included in the analysis ranges from 113 to 143, out of a total of 228 districts.

Results

Modeling the TB fatality rate and objective function

Using upscaled TB data in Eq. (3), we aim to minimize the total number of TB-related deaths by reallocating hospitals across districts while accounting for age-specific effects. To this end, we reformulate the objective function in Eq. (1) by decomposing total fatalities into age-group components. Specifically, the original fatality rate ϕ_s is extended to $\phi_{s,t} \equiv D_{s,t}/N_{s,t}$, representing the fatality rate for age group t in district s . As stated in Eq. (1), the fatality rate was modeled as $\phi_s(\eta_s) = \exp(-\eta_s/\tilde{\eta}_s)$, where η_s denotes the areal density of hospitals and $\tilde{\eta}_s$ represents a district-specific characteristic density. In our age-disaggregated formulation, individuals in district s access a shared set of H_s hospitals regardless of age, implying that the hospital density remains $\eta_{s,t} = \eta_s$. However, hospital accessibility may vary across age groups (e.g., due to differences in mobility and activity), resulting in an age-dependent characteristic density $\tilde{\eta}_{s,t}$. Accordingly, the age-specific fatality rate is modeled as

$$\phi_{s,t} = \exp(-\eta_s/\tilde{\eta}_{s,t}), \quad (4)$$

with the characteristic density empirically estimated as

$$\tilde{\eta}_{s,t} = \frac{\eta_s}{-\log \phi_{s,t}} = \frac{H_s/A_s}{\log(N_{s,t}/D_{s,t})}, \quad (5)$$

using the observed values of $N_{s,t}$, $D_{s,t}$, and H_s summarized in Table 2. This formulation implies that $\tilde{\eta}_{s,t}$ is directly proportional to the hospital density and inversely related to the observed fatality rate. For elderly age groups in districts with insufficient hospital infrastructure, $\tilde{\eta}_{s,t}$ tends to be high, implying that more hospitals are required to reduce fatality rates. Consequently, a comparable reduction in $\phi_{s,t}$ requires a larger increase in hospital density than in districts with better infrastructure and access.

Using the model defined in Eq. (4), the total number of fatalities, which serves as the objective function to be minimized, can be written as a function of hospital densities:

$$E_{\text{fatalities}}(\vec{\eta}) = \sum_{s,t} D_{s,t} = \sum_{s,t} N_{s,t} \phi_{s,t} = \sum_{s,t} N_{s,t} \exp(-\eta_s/\tilde{\eta}_{s,t}). \quad (6)$$

We vary $\vec{\eta}$ to minimize $E_{\text{fatalities}}(\vec{\eta})$ while the total number H of hospitals is preserved. The optimal hospital density $\eta_s^{(\text{opt})}$ that minimizes $E_{\text{fatalities}}(\vec{\eta})$ can, in principle, be obtained analytically using the Lagrange multiplier method. However, when age groups t are taken into account in Eq. (6), a closed-form solution is not available. Therefore, we perform a numerical optimization to determine the optimized hospital configuration vector $\vec{\eta}^{(\text{opt})} = (\eta_1^{(\text{opt})}, \eta_2^{(\text{opt})}, \dots, \eta_s^{(\text{opt})}, \dots)$ using a zero-temperature Monte Carlo approach. A randomly selected pair (u, v) of districts attempts to exchange a small amount of hospital allocation, denoted by ΔH , through the updates $H_u \rightarrow H_u - \Delta H$ and $H_v \rightarrow H_v + \Delta H$. If this relocation results in a decrease in the total fatalities $E_{\text{fatalities}}$, the new configuration is accepted. This process is repeated until $E_{\text{fatalities}}$ converges to a minimum value, denoted by $E_{\text{fatalities}}^{(\text{min})}$. The optimized density configuration is defined as the one that minimizes the objective function, i.e.,

$$E_{\text{fatalities}}^{(\text{min})} \equiv E(\vec{\eta}^{(\text{opt})}). \quad (7)$$

Here we use $\Delta H = 0.01$, which is sufficiently small to ensure the convergence of $E_{\text{fatalities}}^{(\text{min})}$ with respect to ΔH .

To understand the effect of accounting for age-group distributions on the optimization process, we compare the age-considered optimization results to the baseline case studied in the previous work¹¹, which uses the objective function in Eq. (1). We first examine the relative change in hospital density compared to the original empirical density η , specifically $\eta_{\text{age}}^{(\text{opt})}/\eta$ and $\eta_{\times}^{(\text{opt})}/\eta$, which are obtained by minimizing the objective function $E_{\text{fatalities}}$ in Eq. (6) for $\eta_{\text{age}}^{(\text{opt})}$ and $E(\vec{\eta})$ in Eq. (1) for $\eta_{\times}^{(\text{opt})}$, respectively. Here, the subscript \times represents the optimal hospital density obtained without accounting for age-group differences. Since elderly individuals account for a substantial portion of TB patients and fatalities, we analyze the optimization results with respect to the areal patient density of the oldest age group ($t = 5$, ages 80 and above), defined as $\rho_{s,5} = N_{s,5}/A_s$. The relative changes $\eta_{\text{age}}^{(\text{opt})}/\eta$ and $\eta_{\times}^{(\text{opt})}/\eta$ are nearly identical [see the color map in Fig. 4(a) and the y-axis scales in Figs. 4(b) and 4(c)].

A higher density of elderly patients alone does not necessarily lead to a greater hospital allocation in the age-considered optimization [Fig. 4(b)], indicating that absolute patient density is not a sufficient predictor of post-optimization hospital gain. In

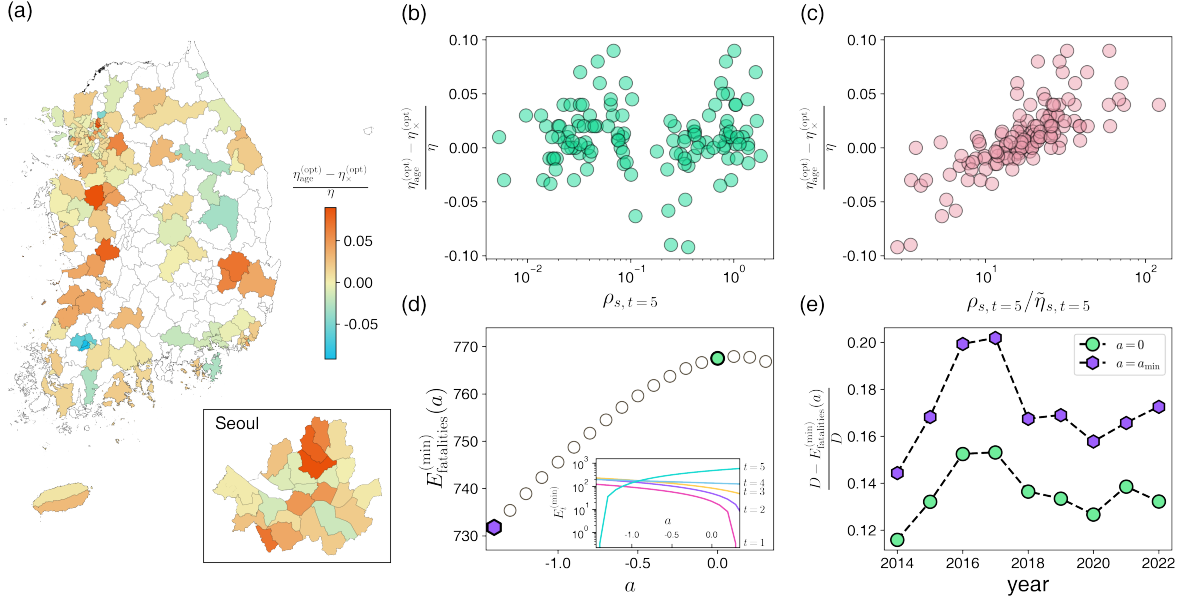


Figure 4. (a) District-level values of the difference $(\eta_{age}^{(opt)} - \eta_x^{(opt)})/\eta$ across South Korea. The inset shows a magnified view of Seoul. Uncolored districts indicate no data satisfying the criteria. (b-c) Comparison of the difference $(\eta_{age}^{(opt)} - \eta_x^{(opt)})/\eta$ for $\rho_{s,5}$ (b) and $\rho_{s,5}/\tilde{\eta}_{s,5}$ (c). No distinct pattern observed along $\rho_{s,5}$, while a steady, roughly linear increase is seen along $\rho_{s,5}/\tilde{\eta}_{s,5}$ despite the log-scaled x-axis. (d) The minimum fatalities $E_{\text{fatalities}}^{(\min)}$ as a function of the age weighting parameter a in 2022 is shown representatively, with $a_{\min} = -1.4$ and $a_{\max} = 0.3$. The purple hexagon and green circle represent the cases of $a = a_{\min}$ and $a = 0$, respectively. The inset figure shows the minimized number of fatalities for each age group t as a function of a . (e) The yearly trend of the deviation of $E_{\text{fatalities}}^{(\min)}$ from the original deaths D when $a = a_{\min}$ and $a = 0$. A bigger value indicates a greater reduction in fatalities compared to the original deaths D . Across all analyzed years, the cases with $a = a_{\min}$ achieve a better reduction in fatalities than those of $a = 0$.

line with Ref.¹¹, which showed that hospital gain or loss is governed by the characteristic patient density, we therefore examine the optimization outcomes from the perspective of the rescaled density $\rho_{s,5}/\tilde{\eta}_{s,5}$. We find that the rescaled patient density plays a dual role. First, the relative change in hospital density $\eta_{age}^{(opt)}/\eta$ exhibits a clear dependence on $\rho_{s,5}/\tilde{\eta}_{s,5}$, indicating that this quantity continues to govern whether a district gains or loses hospitals after optimization [Fig. S1 in the Supplemental Material]. Second, the difference between the age-considered and age-agnostic optimizations, $(\eta_{age}^{(opt)} - \eta_x^{(opt)})/\eta$, is also systematically controlled by the same rescaled density [Fig. 4(c)]. In this sense, the rescaled patient density $\rho_{s,5}/\tilde{\eta}_{s,5}$ governs not only the direction of hospital redistribution after optimization, but also amplifies the difference in hospital gains between the age-considered and age-agnostic cases.

The characteristic scale $\tilde{\eta}_{s,t}$ defined in Eq. (5) is strongly correlated with the age-aggregated scale $\tilde{\eta}_s$, since the empirical fatality rate $\phi_{s,t}$ is constrained by the overall rate ϕ_s . This correlation explains why the behavior of the hospital density difference also mirrors a similar dependence on the age-aggregated ratio $\rho/\tilde{\eta}$ [see Fig. S2 in the Supplemental Material].

The effect of age scaling in total fatalities

The age distribution of TB patients may vary with time depending on societal factors, such as the baby boom generation or population aging. To account for such scenarios, we introduce a simple linear weight of the form $at + b$ applied to the patient counts in Eq. (6). Incorporating this weighting, the objective function for optimization is redefined as follows:

$$E_{\text{fatalities}}(\vec{\eta}; a) = \sum_{s,t} E_{s,t} = \sum_{s,t} (at + b) N_{s,t} \exp(-\eta_s/\tilde{\eta}_{s,t}), \quad (8)$$

which allows us to rewrite the optimal fatalities $E_{\text{fatalities}}^{(\min)}$ in Eq. (7) as a function of a as $E_{\text{fatalities}}^{(\min)} \equiv E(\vec{\eta}^{(opt)}; a)$. We will show later that b is not a free parameter but given by a factor of a . The positive value of a assigns greater weight to older age groups, reflecting an aging society, whereas a negative value emphasizes younger age groups, corresponding to a youthful society scenario. When $a = 0$, the age-weighted objective function $E_{\text{fatalities}}(\vec{\eta}; a = 0)$ in Eq. (8) reduces to the original, unweighted

formulation in Eq. (6). The slope a in the age-weighting function is constrained to lie within a bounded range, $a_{\min} < a < a_{\max}$, in order to avoid unphysical conditions such as negative weighted fatalities for any age group. The bounds are defined as follows:

$$a_{\min} = \min[a \in \mathbb{R} \mid at + b \geq 0 \text{ for all } t \in \{1, 2, 3, 4, 5\}],$$

$$a_{\max} = \max[a \in \mathbb{R} \mid at + b \geq 0 \text{ for all } t \in \{1, 2, 3, 4, 5\}],$$

where \mathbb{R} is the set of real numbers. The optimized fatalities $E_{\text{fatalities}}^{(\min)}$ can be obtained as a function of a for a given year, and the feasible range of a is approximately $-1.4 \lesssim a \lesssim 0.3$ over the nine-year period, as shown in Fig. S3 in the Supplemental Material.

Since the optimization process begins from the empirical number of total fatalities, computed as $D = \sum_{s,t} D_{s,t}$ and listed in Table 2, the parameter b in the age-weighting function is chosen to ensure that $E_{\text{fatalities}}$ evaluated at the empirical $\vec{\eta}$ in Eq. (8) equals the empirical value D for a given a . That is, $\sum_{s,t} (at + b)D_{s,t} = D$ and this condition determines b as a function of a :

$$b(a) = 1 - a \sum_{s,t} t \frac{D_{s,t}}{D}. \quad (9)$$

All quantities on the right-hand side of Eq. (9), except for a , are taken from the original empirical values prior to optimization. The characteristic hospital density is not altered by the age scaling because the fatality rate $\phi_{s,t} = D_{s,t}/N_{s,t}$ entering Eq. (5) remains unchanged.

The behavior of the minimum fatalities $E_{\text{fatalities}}^{(\min)}$ as a function of the age-weighting parameter a is shown in Fig. 4(d), using the year 2022 as a representative case. The curve exhibits a slightly concave shape with a peak near $a = 0$, which is a typical pattern observed across all years. The respective fatalities $E_t^{(\min)}$ for each age group t —leading to $E_{\text{fatalities}}^{(\min)} = \sum_{t=1}^5 E_t^{(\min)}$ —show different behaviors as functions of a . The fatalities $E_5^{(\min)}$ of the oldest group decrease very rapidly with decreasing a for $a < 0$, while those of the other groups increase with decreasing a , as seen in the inset of Fig. 4(d). The behavior of $E_5^{(\min)}$ in the oldest group governs the behavior of $E_{\text{fatalities}}^{(\min)}$. The minimum value is $E_{\text{fatalities}}^{(\min)} = 731.80$ (approximately a 17% decrease from the empirical total $D = 886$) at $a = -1.4 \simeq a_{\min}$, whereas the corresponding value at $a = 0$ is 767.54 (about a 13% decrease). This implies that the reduction in the elderly patients in a youthful society ($a < 0$) would decrease the total fatalities significantly. The tendency $E_{\text{fatalities}}^{(\min)}(a = 0) > E_{\text{fatalities}}^{(\min)}(a \simeq a_{\min})$ is consistently observed across all periods [Fig. 4(e)]. The curve $E_{\text{fatalities}}^{(\min)}$ as a function of a for all periods is displayed in Fig. S3 in the Supplemental Material.

To explore how demographic weighting influences the reallocation of hospitals and its consequences at the district level, we compare two representative scenarios: the empirical baseline with $a = 0$ and a hypothetical youthful society with $a \simeq a_{\min}$. In both cases, the total number of hospitals remains constant, but the optimal allocation patterns differ due to the application of age-dependent weights in the objective function. For each district s , we define the relative changes in hospital allocation and

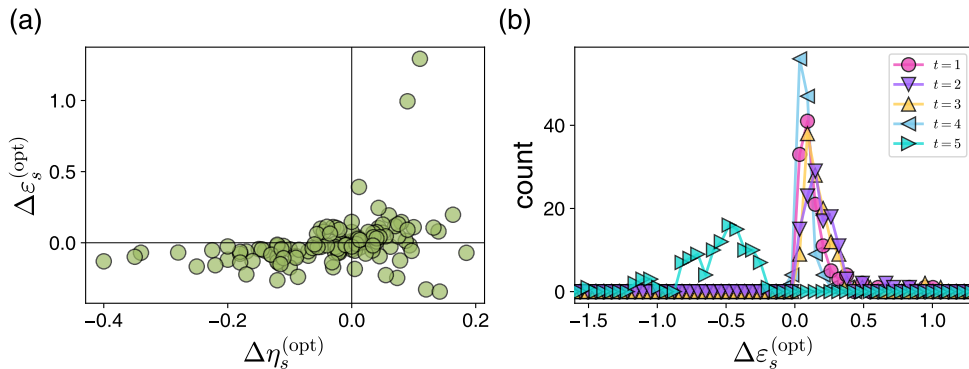


Figure 5. (a) Relationship between relative changes in optimal hospital allocation $\Delta\eta_s^{(\text{opt})}$ versus fatality $\Delta\epsilon_s^{(\text{opt})}$ across districts under the $a \simeq a_{\min}$ case compared to the baseline case ($a = 0$). (b) A distribution of fatality change $\Delta\epsilon_s^{(\text{opt})}$ for age group t . $\Delta\epsilon_s^{(\text{opt})}$ for $t = 5$ (ages 80 and above) concentrated in the negative range, unlike other age groups.

fatalities as follows:

$$\Delta\eta_s^{(\text{opt})} \equiv \frac{\eta_s^{(\text{opt})}(a \simeq a_{\min}) - \eta_s^{(\text{opt})}(a = 0)}{\eta_s}, \quad \Delta\epsilon_s^{(\text{opt})} \equiv \frac{E_s^{(\text{opt})}(a \simeq a_{\min}) - E_s^{(\text{opt})}(a = 0)}{D_s}.$$

These quantities represent, respectively, the relative changes in hospital allocation and total TB fatalities for each district when moving from the baseline to the youthful weighting scenario. Here, the case $a \simeq a_{\min}$ is taken as a representative youthful society, while the opposite extreme case $a \simeq a_{\max}$, corresponding to an aging society, is analyzed separately in Fig. S4 in the Supplemental Material.

Figure 5(a) shows a scatter plot of $\Delta\eta_s^{(\text{opt})}$ versus $\Delta\epsilon_s^{(\text{opt})}$ for all districts. In youthful society, some districts lose hospital resources and exhibit reductions in fatalities, whereas others gain resources and show increases in fatalities. To clarify the origin of these different behaviors, we decompose the total fatality change into age-group-specific contributions, $\Delta\epsilon_t^{(\text{opt})}$ for $t = 1, \dots, 5$ [Fig. 5(b)]. This decomposition reveals a strong asymmetry across age groups. The contribution from the oldest group ($t = 5$, ages 80 and above) is consistently negative across districts, whereas younger age groups typically show small positive contributions. Consequently, the net fatality change in a district is determined by the balance between the reduction in the oldest group and the cumulative increase among younger groups.

This composition helps explain the outcomes observed under age-weighted optimization. In the youthful weighting scenario, some districts receive more hospitals than in the baseline case and still exhibit an increase in total fatalities. This is not because fatalities rise among the elderly, but because increases in younger age groups outweigh the reduction achieved in the oldest group along with increased hospital resources compared with the baseline scenario. The opposite case is understood in the similar manner. These observations indicate that demographic weighting modifies not only the spatial allocation of hospitals but also how allocation changes translate into fatality outcomes. The comparison between age-weighted and baseline optimizations further shows that demographic weighting can substantially alter spatial allocation patterns under fixed infrastructural constraints (as encoded in $\tilde{\eta}_{s,t}$). Rather than responding uniformly to hospital gains or losses, district-level outcomes reflect a competition between reductions in the oldest age group and cumulative increases across younger groups. This sensitivity to age composition emphasizes the importance of interpreting optimization results through age-resolved contributions rather than aggregate fatality metrics alone, and motivates further discussion on demographic effects in healthcare planning.

Discussion

We present a high-resolution dataset that incorporates age-specific tuberculosis (TB) fatality information and detailed hospital distribution in South Korea. The dataset is constructed by integrating age-stratified ‘si’ and ‘do’ level spatial data with non-age-stratified ‘si’, ‘gun’, and ‘gu’ level spatial data, enabling optimization analyses that reflect both demographic vulnerability and spatial variation at the district scale. A key strength of the dataset is that it supports weighted optimization of healthcare infrastructure through an explicit age-weighting scheme. By introducing an age-weighting parameter into the objective function, we systematically examine how different age-weighting scenarios influence the spatial configuration of hospital resources. While different scenarios can yield similar total numbers of minimized fatalities, the resulting hospital distributions may differ substantially depending on the underlying age structure, highlighting the importance of demographic heterogeneity in spatial healthcare allocation.

In the context of TB, a disease that remains a major public health challenge in South Korea, our analysis demonstrates that age structure plays a critical role in determining optimal spatial allocation patterns. We find that increasing hospital resources in a region does not necessarily lead to proportional reductions in fatalities unless age-dependent risk profiles are taken into account. In some regions, reductions in hospital allocation can still coincide with decreased fatalities, reflecting shifts in age burden or pre-existing differences in characteristic hospital density. These results suggest that spatial optimization strategies that ignore demographic composition may overlook important sources of heterogeneity, particularly in aging societies where regional disparities in age structure and fatality risk are pronounced.

Several limitations of this study should be stated. Age-disaggregated TB data at the district level are reconstructed from province-level distributions, which implicitly assumes homogeneous age composition within each province and may obscure finer-scale demographic variation. In addition, hospital accessibility is represented through areal hospital density and does not explicitly account for differences in capacity, quality of care, or transportation infrastructure. As a result, the optimized configurations should be interpreted as relative allocation patterns rather than as direct prescriptions for policy implementation.

Despite these limitations, the framework provides a consistent basis for comparative or exploratory studies of demographic effects in spatial healthcare allocation. Beyond TB, the weighted formulation of the objective function allows the same approach to be applied to other health-related settings, provided that appropriate data are available. Because the objective function is explicitly formulated as a weighted sum over demographic groups, the same framework can be applied to different diseases or risk profiles by modifying the weighting scheme or the definition of fatality risk, provided that appropriate data are available. In

this sense, the dataset can serve as a basis for comparative or exploratory studies rather than as a prescriptive tool for policy design.

Data Availability

The dataset supporting this study has been deposited in the Dryad Digital Repository and is available for peer review at the following private link: <https://datadryad.org/share/qfxSkgpvSxiVsZhnUP8jLxwMMIXUiLwCaVrP5Y0Djek>. This dataset contains annual tuberculosis (TB) statistics across administrative districts in South Korea from 2014 to 2022. It includes district-level counts of hospitals, TB patients, and fatalities, along with age-stratified proportions of new cases and deaths (by 10-year age groups from 0–9 to 80+). The dataset was reconstructed using publicly available provincial-level data from the Korea Disease Control and Prevention Agency (KDCA) and the Korean Statistical Information Service (KOSIS), and harmonized with higher-resolution regional information to produce a novel age-stratified TB dataset. All variables are fully documented in the accompanying metadata and README file. The dataset will be assigned a DOI and made publicly available upon publication.

Code Availability

The code used for data preprocessing, age-stratified fatality modeling, and hospital optimization is openly available at https://github.com/kwyoosu7/Tuberculosis_hospital_distribution_optimization. The repository includes Python scripts for constructing the dataset, implementing optimization routines, and generating the figures used in the manuscript.

References

1. (WHO), W. H. O. Tuberculosis data. <https://www.who.int/tb/data/en/> (2023). Accessed: 2025-04-14.
2. Glaziou, P., Sismanidis, C., Floyd, K. & Raviglione, M. Global epidemiology of tuberculosis. *Cold Spring Harb. perspectives medicine* **5**, a017798 (2015).
3. Renner, A.-T. Hospitals as social infrastructure: accessible for all? In *Handbook of Social Infrastructure*, 20–38 (Edward Elgar Publishing, 2024).
4. Chung, S. *et al.* Access to emergency services: A new york city case study. *Transp. Res. Interdiscip. Perspectives* **25**, 101111 (2024).
5. Lee, H., Kim, J., Kim, J. & Park, Y.-J. Review of the global burden of tuberculosis in 2023: Insights from the who global tuberculosis report 2024. *Public Heal. Wkly. Rep.* **18**, S55–S69 (2025).
6. Korea Disease Control and Prevention Agenc. Available from <https://www.kdca.go.kr> (Accessed: 12.15.2023).
7. Korean Statistical Information Service. Available from <http://kosis.kr> (Accessed: 12.15.2023).
8. Lee, J.-H., Jo, J., Kim, J. W., Lee, K. & Choi, M. Y. Spatial distributions of restaurants emerging from pedestrian behavior and online information sharing. *Phys. A: Stat. Mech. its Appl.* **597**, 127265 (2022).
9. Lee, M. J. & Kim, B. J. Spatial uniformity in the power-grid system. *Phys. Rev. E* **95**, 042316 (2017).
10. Um, J., Son, S.-W., Lee, S.-I., Jeong, H. & Kim, B. J. Scaling laws between population and facility densities. *Proc. Natl. Acad. Sci.* **106**, 14236–14240 (2009).
11. Lee, M. J., Kim, K., Son, J. & Lee, D.-S. Optimizing hospital distribution across districts to reduce tuberculosis fatalities. *Sci. Reports* **10**, 8603 (2020).
12. Gastner, M. T. & Newman, M. E. Optimal design of spatial distribution networks. *Phys. Rev. E* **74**, 016117 (2006).
13. Stephan, G. E. Territorial division: The least-time constraint behind the formation of subnational boundaries. *Science* **196**, 523–524 (1977).
14. Kwon, Y., Lee, M. J. & Son, S.-W. Quantifying traffic patterns with percolation theory: a case study of seoul roads. *J. Korean Phys. Soc.* **86**, 693–700 (2025).
15. Gusein-Zade, S. M. Bunge's problem in central place theory and its generalizations. *Geogr. Analysis* **14**, 246–252 (1982).
16. Kim, D., Son, S.-W. & Jeong, H. Demographic studies of internet routers. *J. Korean Phys. Soc.* **60**, 585–589 (2012).
17. Wuellner, D. R., Roy, S. & D'Souza, R. M. Resilience and rewiring of the passenger airline networks in the united states. *Phys. Rev. E* **82**, 056101 (2010).

18. Thomas, T. Y. & Rajagopalan, S. Tuberculosis and aging: A global health problem. *Clin. Infect. Dis.* **33**, 1034–1039 (2001).
19. Hopewell, P. C., Pai, M., Maher, D., Uplekar, M. & Raviglione, M. C. International standards for tuberculosis care. *The Lancet infectious diseases* **6**, 710–725 (2006).
20. Centers for Disease Control and Prevention. *Core Curriculum on Tuberculosis: What the Clinician Should Know* (Centers for Disease Control and Prevention, Atlanta, GA, 2013).
21. Hughes, B. D. *Random walks and random environments* (Oxford University Press, 1996).

Acknowledgements

This work was supported by the National Research Foundation (NRF) of Korea through Grant Numbers. NRF-2023R1A2C1007523 (S.-W.S.), RS-2024-00341317 (M.J.L.), and by KIAS Individual Grants (No. CG079902 (D.-S.L.)). We thank APCTP, Pohang, Korea, for their hospitality during the Topical Research Program [APCTP-2025-T04], from which this work benefited greatly.

Author contributions statement

Y.K., D.-S.L., M.J.L., and S.-W.S. designed, conceptualized, and wrote the manuscript. Y.K. and M.J.L. searched out and digitized the TB dataset. D.-S.L. assisted with the early generation of the datasets. Y.K. developed and implemented the optimization models, conducted the computational analysis, and also performed the spatial data processing and visualization. D.-S.L., M.J.L., and S.-W.S. supervised the project and provided critical guidance on the methodological framework. All the authors contributed to reviewing and editing the manuscript.

Competing interests

The authors declare no competing interests.

Supplemental Material

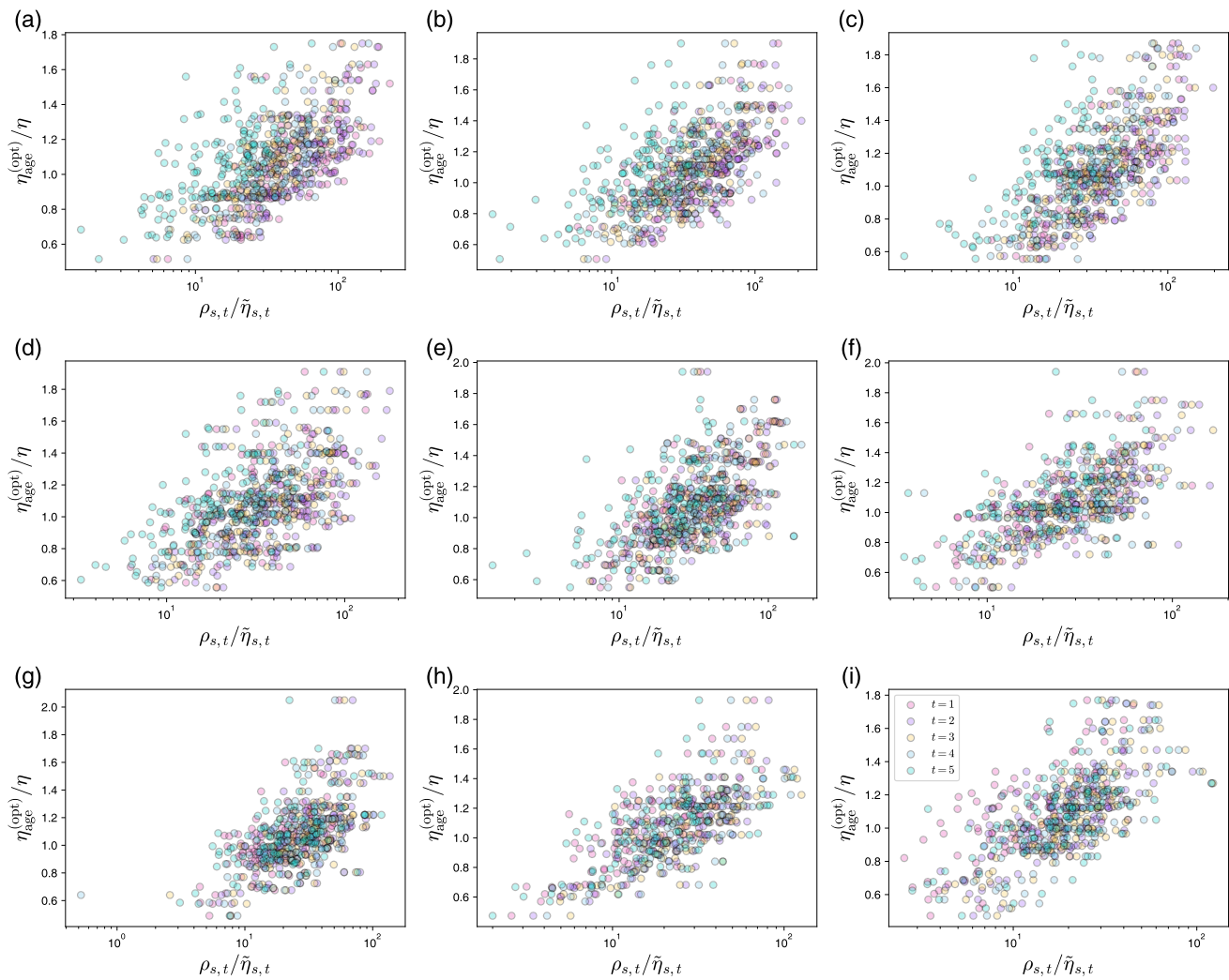


Figure S1. Plot of the ratio $\frac{\eta_{age}^{(opt)}}{\eta}$ versus the rescaled patient density $\frac{\rho_{s,t}}{\bar{\eta}_{s,t}}$ from 2014 to 2022 (a-i). All age groups exhibit an increasing trend along the log-scaled x-axis.

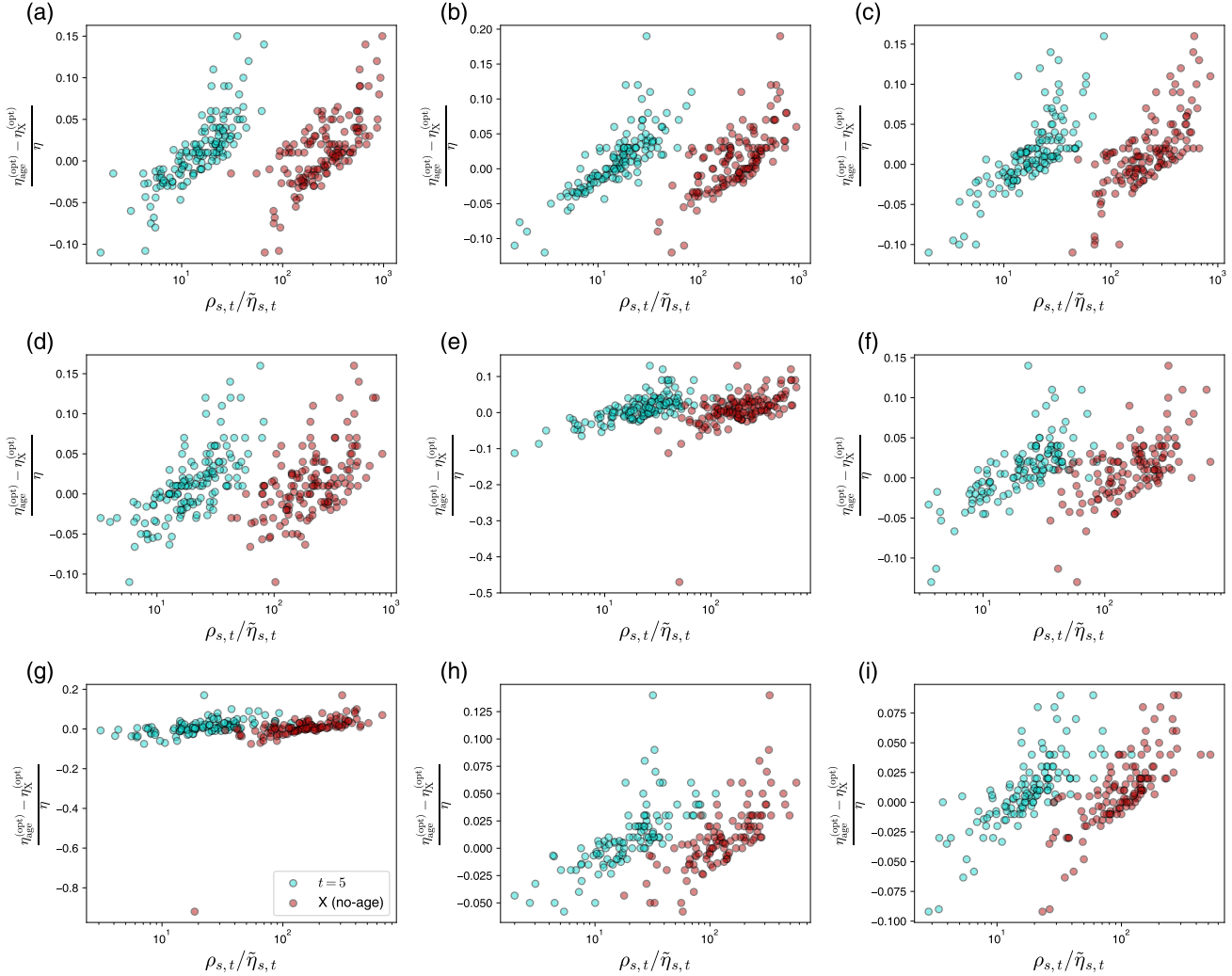


Figure S2. The difference between relative changes in hospital density $\frac{\eta_{age}^{(opt)} - \eta_X^{(opt)}}{\eta}$ versus the rescaled patient density $\frac{\rho_{s,t}}{\tilde{\eta}_{s,t}}$ from 2014 to 2022 (a-i) in $t = 5$ age group and no-age case.

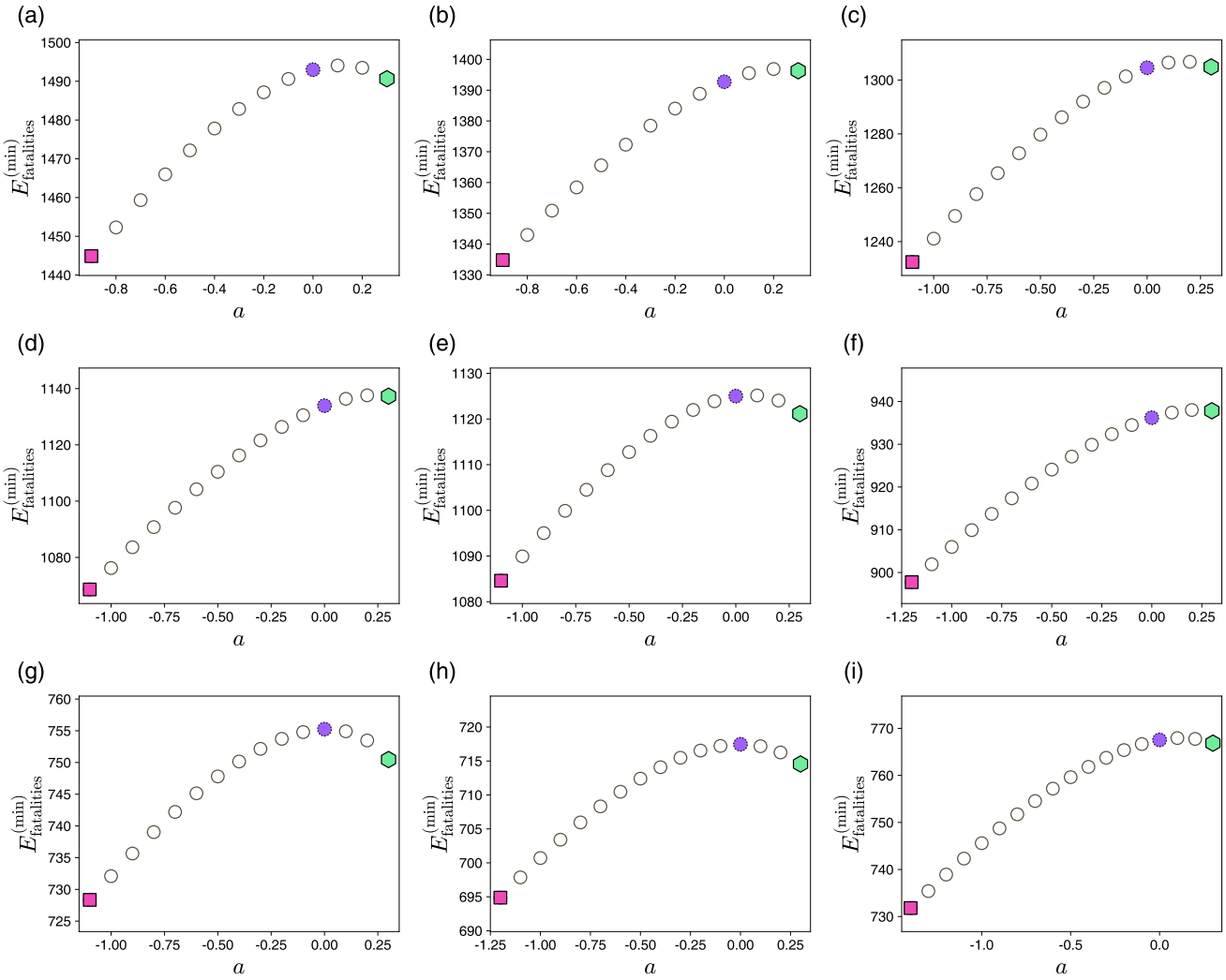


Figure S3. The minimum fatalities $E_{\text{fatalities}}^{(\text{min})}$ as a function of the age weighting parameter a from 2014 to 2022 is shown representatively, with a_{\min} and a_{\max} . The pink square, green hexagon and purple circle represent the cases of $a = a_{\min}$, $a = a_{\max}$ and $a = 0$, respectively.

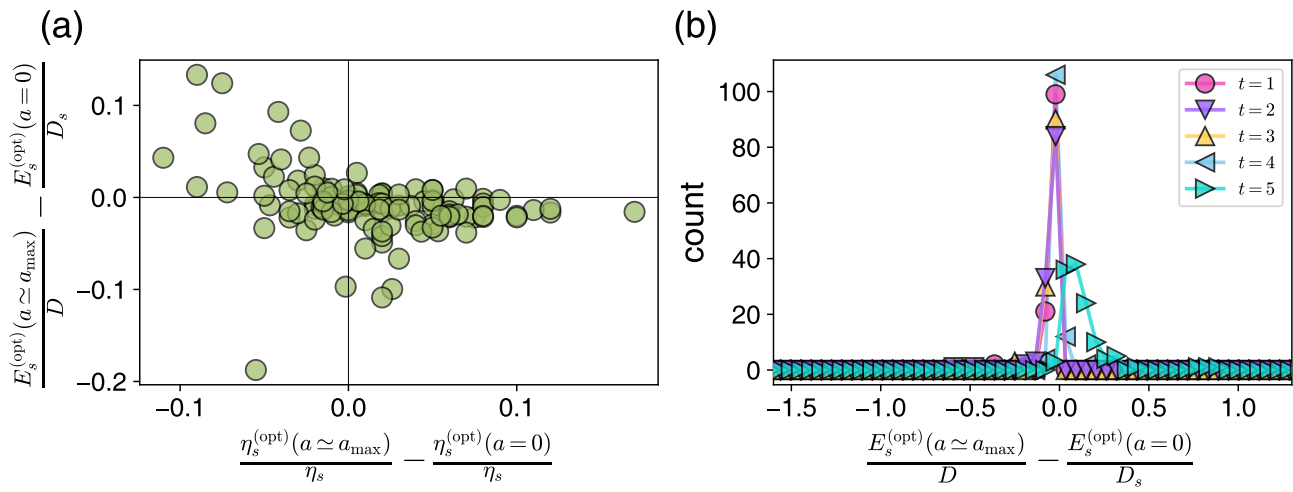


Figure S4. (a) Relationship between relative changes in optimal hospital allocation $\frac{\eta_s^{(\text{opt})}(a \simeq a_{\max})}{\eta_s} - \frac{\eta_s^{(\text{opt})}(a=0)}{\eta_s}$ versus fatality $\frac{E_s^{(\text{opt})}(a \simeq a_{\max})}{D} - \frac{E_s^{(\text{opt})}(a=0)}{D_s}$ across districts under the $a \simeq a_{\max}$ case compared to the baseline case ($a = 0$). (b) A distribution of fatality change $\frac{E_s^{(\text{opt})}(a \simeq a_{\max})}{D} - \frac{E_s^{(\text{opt})}(a=0)}{D_s}$ for age group t . $\frac{E_s^{(\text{opt})}(a \simeq a_{\max})}{D} - \frac{E_s^{(\text{opt})}(a=0)}{D_s}$ for $t = 5$ (ages 80 and above) concentrated in the negative range, unlike other age groups.